NIH Public Access
Author Manuscript
Heart Rhythm. Author manuscript; available in PMC 2014 November 01.

Published in final edited form as:
Heart Rhythm. 2013 November ; 10(11): . doi:10.1016/j.hrthm.2013.08.010.

Transmural $I_{K(ATP)}$ Heterogeneity as a Determinant of Activation Rate Gradient During Early Ventricular Fibrillation: Mechanistic Insights from Rabbit Ventricular Models

Patrick M Boyle, PhD[1,2], **Stéphane Massé, MASc**[3], **Kumaraswamy Nanthakumar, MD**[3], and **Edward J Vigmond, PhD**[1,4]

[1]University of Calgary, Calgary, Canada

[2]Institute for Computational Medicine, Johns Hopkins University, Baltimore, USA

[3]University Health Network, Toronto, Canada

[4]Institut LIRYC, Université Bordeaux 1, Bordeaux, France

Abstract

Background—Activation rate (AR) gradients develop during VF with the highest AR on the surface near Purkinje system (PS) terminals (endocardium in humans and rabbits, epicardium in pigs). Application of glibenclamide to block ATP-sensitive potassium current ($I_{K(ATP)}$) prior to VF induction eliminates transmural AR gradients and prevents the induction of sustained arrhythmia. It remains unclear whether the PS, which is resistant to ischemia, is also a factor in AR heterogeneity.

Objective—We sought to dissect $I_{K(ATP)}$ and PS contributions to AR gradients during VF using detailed computer simulations.

Methods—We constructed rabbit ventricular models with either sub-endocardial or sub-epicardial PS terminals. Physiologically relevant $I_{K(ATP)}$ gradients were implemented and early VF was induced and observed.

Results—Prominent AR gradients were only observed in models with large $I_{K(ATP)}$ gradients. The critical underlying factor of AR gradient maintenance was refractoriness in low-$I_{K(ATP)}$ regions, which blocked propagation of action potentials from high-$I_{K(ATP)}$ regions. The PS played no role in transmural AR gradient maintenance, but did cause local spatial heterogeneity of AR on the surface adjacent to terminals. Simulated glibenclamide application *during VF* led to spontaneous arrhythmia termination within a few seconds in most cases. This builds on previous experimental findings of anti-VF properties of glibenclamide pretreatment.

Conclusion—Differential $I_{K(ATP)}$ across the ventricular wall is an important factor underlying AR gradients during VF; thus, higher epicardial AR in pigs is most likely due to an abundance of

© 2013 The Heart Rhythm Society. Published by Elsevier Inc. All rights reserved.

Corresponding Author: PM Boyle, Phone: 443-838-1203, Fax: 410-516-5294, pmjboyle@jhu.edu, Mail: 3400 N Charles St – 316 Hackerman Hall – Baltimore MD 21218 – USA.

Publisher's Disclaimer: This is a PDF file of an unedited manuscript that has been accepted for publication. As a service to our customers we are providing this early version of the manuscript. The manuscript will undergo copyediting, typesetting, and review of the resulting proof before it is published in its final citable form. Please note that during the production process errors may be discovered which could affect the content, and all legal disclaimers that apply to the journal pertain.

Conflicts of interest:
PMB, SM, and KN have nothing to declare.
EJV is President of Cardiosolv LLC.

NIH-PA Author Manuscript
NIH-PA Author Manuscript
NIH-PA Author Manuscript

NIH-PA Author Manuscript

NIH-PA Author Manuscript

NIH-PA Author Manuscript

epicardial $I_{K(ATP)}$. For terminating early VF, our results suggest $I_{K(ATP)}$ modulation is a stronger target than Purkinje ablation.

Keywords

ventricular fibrillation; activation rate; transmural heterogeneity; ATP-sensitive potassium current; Purkinje system

Introduction

Ventricular fibrillation (VF) is an important cause of sudden death but underlying mechanisms that maintain VF early and late after onset are not completely understood. During VF, coronary perfusion ceases, causing global ischemia. This leads to acute electrical remodeling at the level of ventricular myocytes, increasing action potential duration (APD) heterogeneity, a factor thought to be crucial in maintaining reentrant circuits underlying VF.[1]

Experiments in pig ventricles have described regional activation rate (AR) differences during VF, with higher epicardial compared to endocardial AR.[2] An AR gradient (ΔAR) also develops after several minutes of VF in myopathic human hearts, but higher rates are located endocardially.[3] This ΔAR has been linked to elevated subendocardial ATP-sensitive potassium current ($I_{K(ATP)}$).[4] In late phases of long-duration VF in canines, the ECG remains chaotic despite well-defined periods of highly synchronized endocardial activation; triggered activity from the Purkinje system (PS) has been identified as a likely underlying cause.[5] Understanding mechanisms by which adjoining cardiac regions become uncoordinated or completely decoupled could help devise therapies to modulate the maintenance of VF after onset.

Interestingly, elevated AR during VF correlates not only with high $I_{K(ATP)}$ but also with the transmural location of Purkinje-myocardial junctions (PMJs). In humans, the PS terminates in the sub-endocardium, the high-AR region during VF; conversely, in pigs, PS fibers penetrate transmurally to form PMJs in the high-AR sub-epicardium. In dogs, which have sub-endocardial PMJs like humans, chemical ablation of the PS and nearby endocardium abolishes AR during VF and promotes termination.[6]

Thus, as summarized in Fig. 1, it remains unclear whether ΔAR observed during long-duration VF is a consequence of regional $I_{K(ATP)}$ heterogeneity, activity related to the penetrated PS, or some synergistic combination of the two. Since abolishing ΔAR leads to VF termination in myopathic hearts, understanding the source of ΔAR will help define therapeutic targets. Attempts to fully resolve this important question have been hampered by the lack of an in vitro technique for silencing only the PS – chemical ablation of the PS with Lugol's solution destroys several hundred micrometers of endocardium.[6] Thus, despite the importance of understanding VF maintenance, the relative contributions of these two factors to transmural AR heterogeneity remain unknown.

In this study, we use biophysically-detailed computer models to test whether ΔAR during VF can be maintained by $I_{K(ATP)}$-mediated transmural differences in intrinsic APD in the absence of other potentially confounding factors. In particular, we test the hypothesis that experimentally-observed epicardial-to-endocardial ΔAR in pigs must be supported by a relative abundance of $I_{K(ATP)}$ expression on the epicardium. VF is induced with and without PS to assess whether ΔAR is affected by PMJs near the high-AR surface. In addition, we determine which would be the stronger target for terminating VF – modulation of $I_{K(ATP)}$-mediated transmural differences or PS-mediated heterogeneity.

NIH-PA Author Manuscript

NIH-PA Author Manuscript

NIH-PA Author Manuscript

2. Methods

2.1 Computer Model of Ventricles and PS

This study used a finite element model of rabbit ventricles that has been extensively validated and applied by our group.[7-10] Ionic kinetics in ventricular cells were governed by the Mahajan model[11] with a guinea pig-derived ATP-sensitive potassium current ($I_{K(ATP)}$)[12] added. We did not model epicardial/M-cell/endocardial heterogeneity in the myocardium because our goal was to examine $I_{K(ATP)}$ gradient effects in the absence of all other transmural factors.

The PS model was an anatomically-based branching network.[10] As illustrated in Fig. 2A, two geometric variants of the PS were used, with PMJs situated either sub-epicardially or sub-endocardially, approximating ungulate and non-ungulate physiology, respectively. PS ionic properties were described by the Aslanidi model.[13]

2.2 Ischemia Model

To simulate global ischemia, we modified a regional ischemia model.[14] Ventricular cells had sodium and L-type calcium channel conductances decreased by 10% and extracellular potassium concentration ($[K^+]_e$) was elevated to 8.84mM. Since we were interested in modeling early VF, these changes correspond to the 4-minute values in the Tice model with three exceptions: (1) Lateral border zones were removed, since they do not exist in global ischemia;[6] (2) the $[K^+]_e$ gradient was removed, since we sought to investigate the effects of $I_{K(ATP)}$ as the only transmural ionic heterogeneity; and (3) $I_{K(ATP)}$ levels were an independently controlled factor. Ischemic effects were not considered in PS cells, which are more resilient due to higher glycogen stores.[15, 16]

We ran simulations with three $I_{K(ATP)}$ levels, modulated by adjusting the fraction of channels in the active state (f_{ATP}): low (f_{ATP}=0.001%), medium (f_{ATP}=0.112%), and high (f_{ATP}=0.180%). These values were based on single cell dynamic restitution simulations used to calculate the shortest possible APD (maximum AR): for low $I_{K(ATP)}$, restitution characteristics were the same as in the unmodified model; for high $I_{K(ATP)}$, single cells sustained APDs as brief as 80ms, the shortest APs optically mapped epicardially in fibrillating rabbit hearts.[17] The medium $I_{K(ATP)}$ value was chosen such that APD abbreviation was ≈50% as severe as for high $I_{K(ATP)}$. APs in non-ischemic and ischemic cells are shown in Figs. 3A&B; hyperpolarization occurred in high-$I_{K(ATP)}$ ischemic cells, as observed in vitro.[18] Fig. 3C shows restitution curves in ischemic cells.

Endocardial and epicardial $I_{K(ATP)}$ levels were assigned (Fig. 2B) and transmural values were linearly interpolated. 12 combinations were not used since models with lower $I_{K(ATP)}$ on the surface with PMJs were irrelevant to the study.

2.3 Electrogram Recovery/Analysis

Extracellular potential values were differenced to construct pseudo-ECGs as described previously;[8] paired LV endocardial and epicardial recording sites emulated basket catheters and electrode socks (Fig. 2C). On each surface, there were 5 splines with 8 sites each; bull's eye plots were reconstructed accordingly.

During VF, AR was directly measured using transmembrane voltage (V_m) from the nearest myocardial point by counting activations using a −20mV threshold with a 40ms blanking interval. To validate our chosen method, we also calculated ARs with a commonly-used FFT-based approach;[19] our method had considerably less variance.

NIH-PA Author Manuscript

NIH-PA Author Manuscript

NIH-PA Author Manuscript

To quantify spatial heterogeneity of AR distributions within each bull's eye plot, Moran's I was calculated (see the Online Supplement for details). Moran's I values vary from −1 (perfect dispersion) to +1 (perfect uniformity); 0 indicates a statistically random pattern.

2.4 Simulation Protocol

Reentry was induced using an S1-S2 protocol.[9] Initial conditions were obtained by pacing single cell models to quasi-steady state (20 beats, 500ms intervals). Two cycles of His stimulation were simulated in the organ-scale model, the second of which was S1. S2 was a large electric field parallel to the septum 120 to 140ms after S1 (Fig. 2D). For each model, S2 timing was adjusted to induce sustained arrhythmia. This yielded ≈4s of chaotic VF to determine AR. We simulated an additional 5s for each model, with and without $I_{K(ATP)}$ blockade to simulate glibenclamide application. Fig. 2E summarizes the simulation protocol.

3. Results

Sustained (>4s) VF was induced in all models except those in which epicardial and endocardial $I_{K(ATP)}$ were both low; in those cases, reentry terminated spontaneously after ~300ms, regardless of S2 timing. Following each VF-inducing S2, macroscopic reentry around the septum quickly degenerated due to wavebreak and excitation became highly disorganized; these arrhythmias were classified as VF since activity was driven by multiple wavefronts, spatial activation patterns varied considerably from cycle to cycle, and pseudo-ECGs were similar to chaotic ECGs observed clinically in VF.

3.1 Heterogeneous $I_{K(ATP)}$ Expression Underlies Transmural ΔAR During VF

Epicardial and endocardial ARs are tabulated for all simulations in Table 1. Significant transmural ΔAR (>10%) was only observed when $I_{K(ATP)}$ was low on one surface and medium or high on the other. This suggests that relatively long APs in low-$I_{K(ATP)}$ regions led to local conduction block of transmural propagation. The highest ARs overall occurred in models with high $I_{K(ATP)}$ throughout the heart; when a transmural difference was incorporated, global average frequency was reduced due to electrotonic interactions. Notably, the presence or absence of the PS did not play any consistent role in determining AR.

Fig. 4A shows epicardial and endocardial V_m maps during VF with high $I_{K(ATP)}$ on both surfaces and no PS. This resulted in numerous narrow wavefronts throughout the heart, including many instances where points on either side of the wall were excited by the same wavefronts. AR maps (see Fig. 2C for specific locations) were homogeneous, reinforcing the observation of high AR similarity throughout the myocardium.

In contrast, when the same analysis was applied during VF with high epicardial f_{ATP} and low endocardial f_{ATP} (Fig. 4B), a significant transmural ΔAR was observed. Narrow wavefronts were observed epicardially as in A, but the lack of endocardial APD abbreviation resulted in broad regions of simultaneous excitation on that surface. Heterogeneous distributions of refractoriness between the surfaces gave rise to frequent epicardial-to-endocardial conduction block, resulting in uncoordinated activation sequences. AR plots showed dramatic ΔAR; notably, the high-$I_{K(ATP)}$ epicardium activated more slowly in B compared to A (12.1 vs. 13.4Hz), suggesting that the slower-activating, low-$I_{K(ATP)}$ endocardium exerted considerable electrotonic influence in B.

Maintenance of ΔAR by transmural conduction block was further investigated in Fig. 5, which shows V_m traces at 3 points in the ventricular wall (A) and sequential V_m spatial maps for several intervals (B-D). This model had the same $I_{K(ATP)}$ gradient as in Fig. 4B but also had a PS with sub-epicardial endpoints. Intervals from (A) were carefully selected to

NIH-PA Author Manuscript

NIH-PA Author Manuscript

NIH-PA Author Manuscript

show how intrinsically longer APs on the low-$I_{K(ATP)}$ endocardium led to transmural conduction block. The effect on ΔAR is most obvious in (A), where there is clearly a "missing" AP in the endocardial recording (red) during cycle (B) following the extremely long AP in cycle (A). Independent of all model variations, including whether a PS was included, this transmural conduction block was the only factor consistently identified as the underlying basis for ΔAR establishment.

3.2 The PS Affects Spatial AR Distribution During VF

Activity near PMJs clearly modulated V_m organization during VF. As shown in previous model-based research, conductive tissue can interact with working myocardium during reentry in many different ways: refractory ventricular myocytes surrounding PMJs can provide anchoring points for rotors and initiate wavefront fractionation, causing rotors to split and contributing to VF complexity.[9] Additionally, in models where high-$I_{K(ATP)}$ regions were colocalized with PS terminals, narrow wavefronts commonly passed over PMJs; in some circumstances, this resulted in local refractoriness gradients, leading to unidirectional conduction block during PS-to-myocardium propagation. We observed these phenomena frequently in models with the PS; several examples can be seen in in Supplementary Movies 3&4.

In spite of the added complexity of reentry resulting from these effects, the PS did not play an important role in driving transmural ΔAR. However, analysis of reentrant VF did reveal an interesting phenomenon – in the vicinity of PMJs, electrotonic interaction with the PS often resulted in intervals during which myocardial APs were abbreviated or completely suppressed. This locally reduced AR without affecting AR in adjacent myocardial regions, as shown in Figs. 6A&C (compare V_m recordings proximal and distal to PMJ – red vs. blue & black traces). This observation was quantitatively confirmed by calculating Moran's I for the AR plots in question (Figs. B&D); in a total of 4 models including the PS, local spatial distribution of AR on the surface near PMJs was near-random (Moran's I≈0). There was no apparent connection between this phenomenon and $I_{K(ATP)}$ expression gradient.

3.3 $I_{K(ATP)}$ Blockade Leads To VF Termination

To elucidate how $I_{K(ATP)}$ block relates to arrhythmia termination, we simulated transient glibenclamide application during sustained VF. As shown in Fig. 7A, when $I_{K(ATP)}$ was blocked, global AR dropped abruptly and VF terminated spontaneously within 5s in 15 of 20 cases (75%). In contrast, there was only one instance of VF termination (5%) when $I_{K(ATP)}$ levels were unchanged; notably, the pseudo-ECG signals and V_m patterns for the treatment and control versions of that particular model were identical, suggesting that VF was on the verge of spontaneous termination *prior to* drug application. The time between $I_{K(ATP)}$ block and VF termination in the treatment group was variable, with no apparent relationship to $I_{K(ATP)}$ or PS type (Fig. 7B). Figs. 7C&D show V_m maps and ECG recordings for control (top) vs. treatment (bottom) in the same model, with snapshots separated by 50ms starting from 25ms after simulated drug application.

4. Discussion

This study used biophysically-detailed rabbit ventricular computer models to elucidate the relative contributions of $I_{K(ATP)}$ expression gradient and PS effects to the maintenance of AR heterogeneity in early VF. The simulation platform allowed these factors to be dissected, isolated, and examined mechanistically. Our results indicate an appreciable transmural ΔAR during early VF is most readily produced by a large intrinsic transmural APD gradient due to $I_{K(ATP)}$ channel expression heterogeneity. This supports our hypothesis that epicardial-to-

NIH-PA Author Manuscript

NIH-PA Author Manuscript

NIH-PA Author Manuscript

endocardial AR gradients observed during early VF in pigs are caused by an abundance of epicardial $I_{K(ATP)}$, which can be validated in vitro.

Consistent with in vitro findings, we were unable to induce sustained VF in hearts that were either non-ischemic[20] or ischemic with globally low $I_{K(ATP)}$ (a model of pre-treatment with glibenclamide).[4, 21] Moreover, transient $I_{K(ATP)}$ blockade *during VF* was shown to terminate arrhythmias. We speculate that the primary mechanism underlying this pharmacological defibrillation is an overall increase in wavelength rather than elimination of heterogeneity, since there was no difference in efficacy between cases with and without heterogeneous transmural $I_{K(ATP)}$ expression and/or large ΔAR. This is consistent with the experimentally-observed response to glibenclamide pre-treatment, which showed a marked slowing of VF in addition to decreased heterogeneity;[4] the global APD prolongation that underlies this slowing of VF has the greatest effect among factors that reduce APD variability.[22]

The simulation platform enables fine-grain control of the $I_{K(ATP)}$ gradient, which allowed quantification of the required transmural difference to achieve significant ΔAR. Channel block and augmentation are also precisely specified, which cannot be achieved pharmacologically.[23] Since $I_{K(ATP)}$ expression level is the only transmural heterogeneity in our model, simulations isolate its pronounced AP shortening effect from all other ischemic factors. This allows us to exclude the PS as a factor in the establishment and maintenance of ΔAR during early VF.

4.1 $I_{K(ATP)}$ Gradient Effects

Incorporation of transmural $I_{K(ATP)}$ gradients resulted in ΔAR of up to 32.60%. The most obvious mechanism responsible was transmural conduction block due to intrinsically longer APs on the low-$I_{K(ATP)}$ surface, which gave rise to broadened wavefronts. These surfaces are also more likely to undergo full-blown APs, since blocked propagation creates a large excitable gap that will be engulfed by the next propagating wavefront. This is elegantly illustrated by the transition between intervals C&D in Fig. 5.

This study was conducted in a rabbit ventricular model because it has been subjected to rigorous validation, especially in terms of its characterization of PMJ dynamics.[7-10] Moreover, VF in rabbits is the closest to human VF in terms of organization.[24] However, the thin walls of the rabbit ventricles introduce certain limitations vis-à-vis transmural heterogeneity. For example, in the published ischemia model, sub-endocardial f_{ATP} is set to 60% of the sub-epicardial peak.[14] In the case of epicardial f_{ATP}=0.180% in this study, this yields endocardial f_{ATP}=0.108%, which is close to our “medium” value, 0.112%. With this transmural $I_{K(ATP)}$ gradient, there is no appreciable ΔAR (see Table 1) because electrotonic smoothing has a strong effect in the thin lapine myocardial walls. In larger hearts (e.g., human or pig), the same intrinsic APD differences might result in appreciable ΔAR due to increased ventricular wall thickness. This emphasizes the need to develop geometrically- and physiologically-detailed models of the human and pig ventricles *including the PS*.

4.2 PS Effects

The role of the PS in promoting transmural AR heterogeneity during early VF (up to 4 minutes post-onset) appears quite limited, but alteration of dynamics near PMJs does affect local activation patterns. In several cases, the PS caused increased local heterogeneity of AR. This finding is of limited interest to the objective of this study, but the PS clearly plays a role in modulating VF dynamics. Our PS geometry is simplistic and PMJ transmission behavior is phenomenological;[7] a more realistic PS model might amplify conduction system contributions to regional ΔAR heterogeneity to the point where transmural ΔAR is significantly affected. In particular, increasing PMJ density and incorporating

NIH-PA Author Manuscript

NIH-PA Author Manuscript

NIH-PA Author Manuscript

autorhythmicity or ectopy might result in more breakthroughs on the high-$I_{K(ATP)}$ surface, further elevating local AR.

A major effect of the PS is functional elongation of APD in coupled ventricular myocytes. We speculate that this behavior may be responsible for islands of long APD (so-called "max" cells) observed subendocardially in non-failing human hearts.[25] During VF, our models show that these regions of prolonged APD have competing effects with regards to the complexity of reentrant activity – rotor anchoring increases VF organization while wavefront fractionation makes patterns more disorderly. As such, it is unclear whether the loss of heterogeneity seen in failing hearts will be anti- or pro-arrhythmic with regards to these particular effects.

Massé et al. observed an increased number of wavebreaks on the epicardium of human hearts during VF.[3] Our simulations suggest that this is not related to breakthroughs from originating from PS excitations; rather, we speculate that these wavebreaks may occur because low-$I_{K(ATP)}$ surfaces have larger excitable gaps due to long pauses following blocked APs, increasing the propensity for breakthroughs. In contrast, high-$I_{K(ATP)}$ surfaces operate near the minimum APD with little or no delay between repolarization and re-excitation; thus, although PMJs tend to be located near these surfaces, it is unlikely that activations emanating from the PS will disrupt nearby persistent reentrant wavefronts. This provides another reason why the PS does not play an important role in maintaining ΔAR in these simulations of VF.

Interestingly, we observed numerous intervals of "ping-pong" behavior in the PS,[26] where excitations in the left and right PS arborizations are out of phase because retrograde impulses never traverse the left-right divide at the His bundle (see Supplementary Movie 5). Thus, instead of one period of relatively synchronous PMJ activation, two shorter intervals are observed. This pattern of behavior does not increase local ARs since total ventricular activation is simply split in two; nor does it significantly alter Moran's I, since activity remains coherent within each ventricle, in spite of a loss of left-right coordination. Further discussion is provided in the Online Supplement.

4.3 Model Limitations

Although these results demonstrate the importance of an intrinsic APD difference to the formation of transmural ΔAR, they do not purport to be a comprehensive investigation of the phenomenon. Indeed, analysis of VF simulations is limited to a small subset of the parameter space representing relatively extreme cases. Future studies should attempt to identify threshold levels of single-cell difference to overcome local electrotonic smoothing effects and give rise to organ-scale heterogeneity. Furthermore, some physiological details, including subepicardial PS penetration and enhanced epicardial $I_{K(ATP)}$ expression, may have different effects when simulated in the context of pig electrophysiology and geometry. In particular, the increase in organ size might promote transmural rate gradients for lower APD differences.[23]

Our model of ischemia was relatively simplistic. Our assumption of a non-ischemic PS during early VF is supported in vivo, but effects on PMJ dynamics are unknown. Increased triggered activity in the myocardium was not simulated because we assumed that once VF is established, reentrant wavefronts mask ectopic activations due to continual excitation. Conduction slowing occurred as a secondary consequence of reduced sodium current; further slowing due to connexin 43 downregulation might qualitatively change reentrant VF patterns but would not affect the overall findings pertaining to the relative importance of $I_{K(ATP)}$ gradients. Finally, our decision to use fixed $[K+]_e$ levels throughout the myocardium is unrealistic, since regional $I_{K(ATP)}$ heterogeneity is one reason why a gradient in $[K+]_e$

NIH-PA Author Manuscript

NIH-PA Author Manuscript

NIH-PA Author Manuscript

forms in the first place. Nonetheless, when restitution curves were recalculated with realistic $[K+]_e$, the medium- and high-$I_{K(ATP)}$ cases hardly changed and the low-$I_{K(ATP)}$ case shifted towards a region of even longer APD. Since the primary finding is that long APs on low-$I_{K(ATP)}$ surfaces sustain ΔAR by promoting transmural conduction block, it is reasonable to expect that incorporating realistic $[K+]_e$ gradients would not qualitatively alter the results.

Our model did not incorporate LV-RV differences in $I_{K(ATP)}$ expression that were recently shown to underlie LV-RV differences in refractoriness during VF.[27] It is unclear whether this heterogeneity might affect transmural ΔAR; this will require further investigation. Notably, since we only examined LV electrogram pairs, it is unlikely that modeling LV-RV heterogeneity would have produced qualitatively different findings.

Supplementary Material

Refer to Web version on PubMed Central for supplementary material.

Acknowledgments

This research was supported by NSERC, the Mprime NCE, NIH NHLBI grant R01HL101196, and Agence National de la Recherche grant ANR-10-IAHU-04 (France).

Glossary

APD	action potential duration
AR	activation rate
$I_{K(ATP)}$	ATP-sensitive potassium current
PS	Purkinje system
PMJ	Purkinje-myocardial junction

References

1. Furukawa T, Kimura S, Furukawa N, Bassett AL, Myerburg RJ. Role of cardiac ATP-regulated potassium channels in differential responses of endocardial and epicardial cells to ischemia. Circ Res. 1991; 68:1693–1702. [PubMed: 2036719]
2. Nanthakumar K, Huang J, Rogers JM, et al. Regional differences in ventricular fibrillation in the open-chest porcine left ventricle. Circ Res. 2002; 91:733–740. [PubMed: 12386151]
3. Massé S, Farid T, Dorian P, et al. Effect of global ischemia and reperfusion during ventricular fibrillation in myopathic human hearts. Am J Physiol Heart Circ Physiol. 2009; 297:H1984–H1991. [PubMed: 19820201]
4. Farid TA, Nair K, Massé S, et al. Role of KATP channels in the maintenance of ventricular fibrillation in cardiomyopathic human hearts. Circ Res. 2011; 109:1309–1318. [PubMed: 21980123]
5. Robichaux RP, Dosdall DJ, Osorio J, et al. Periods of highly synchronous, non-reentrant endocardial activation cycles occur during long-duration ventricular fibrillation. J Cardiovasc Electrophysiol. 2010; 21:1266–1273. [PubMed: 20487123]
6. Cha YM, Uchida T, Wolf PL, et al. Effects of chemical subendocardial ablation on activation rate gradient during ventricular fibrillation. Am J Physiol Heart Circ Physiol. 1995; 269:H1998–H2009.
7. Boyle PM, Deo M, Plank G, Vigmond EJ. Purkinje-mediated effects in the response of quiescent ventricles to defibrillation shocks. Ann Biomed Eng. 2010; 38:456–468. [PubMed: 19876737]
8. Boyle PM, Veenhuyzen GD, Vigmond EJ. Fusion during entrainment of orthodromic reciprocating tachycardia is enhanced for basal pacing sites but diminished when pacing near Purkinje system end points. Heart Rhythm. 2013; 10:444–451. [PubMed: 23207137]

NIH-PA Author Manuscript

NIH-PA Author Manuscript

NIH-PA Author Manuscript

9. Deo M, Boyle P, Plank G, Vigmond E. Arrhythmogenic mechanisms of the Purkinje system during electric shocks: a modeling study. Heart Rhythm. 2009; 6:1782–1789. [PubMed: 19959130]
10. Vigmond EJ, Clements C. Construction of a computer model to investigate sawtooth effects in the Purkinje system. IEEE Trans Biomed Eng. 2007; 54:389–399. [PubMed: 17355050]
11. Mahajan A, Shiferaw Y, Sato D, et al. A rabbit ventricular action potential model replicating cardiac dynamics at rapid heart rates. Biophys J. 2008; 94:392–410. [PubMed: 18160660]
12. Ferrero JJM, Sáiz J, Ferrero JM, Thakor NV. Simulation of action potentials from metabolically impaired cardiac myocytes. Role of ATP-sensitive K+ current. Circ Res. 1996; 79:208–221. [PubMed: 8755997]
13. Aslanidi OV, Sleiman RN, Boyett MR, Hancox JC, Zhang H. Ionic mechanisms for electrical heterogeneity between rabbit Purkinje fiber and ventricular cells. Biophys J. 2010; 98:2420–2431. [PubMed: 20513385]
14. Tice BM, Rodríguez B, Eason J, Trayanova N. Mechanistic investigation into the arrhythmogenic role of transmural heterogeneities in regional ischaemia phase 1A. Europace. 2007; 9(Suppl 6):vi46–vi58. [PubMed: 17959693]
15. Wit AL, Friedman PL. Basis for ventricular arrhythmias accompanying myocardial infarction: alterations in electrical activity of ventricular muscle and Purkinje fibers after coronary artery occlusion. Archives of internal medicine. Mar.1975 135:459–472. [PubMed: 1130921]
16. Dosdall DJ, Tabereaux PB, Kim JJ, et al. Chemical ablation of the Purkinje system causes early termination and activation rate slowing of long-duration ventricular fibrillation in dogs. Am J Physiol Heart Circ Physiol. Aug.2008 295:H883–889. [PubMed: 18586887]
17. Harada M, Tsuji Y, Ishiguro YS, et al. Rate-dependent shortening of action potential duration increases ventricular vulnerability in failing rabbit heart. Am J Physiol Heart Circ Physiol. 2011; 300:H565–H573. [PubMed: 21148762]
18. Gasser RN, Vaughan-Jones RD. Mechanism of potassium efflux and action potential shortening during ischaemia in isolated mammalian cardiac muscle. J Physiol. Dec.1990 431:713–741. [PubMed: 2129231]
19. Zaitsev AV, Berenfeld O, Mironov SF, Jalife J, Pertsov AM. Distribution of excitation frequencies on the epicardial and endocardial surfaces of fibrillating ventricular wall of the sheep heart. Circ Res. 2000; 86:408–417. [PubMed: 10700445]
20. Manoach M, Netz H, Erez M, Weinstock M. Ventricular self-defibrillation in mammals: age and drug dependence. Age and Aging. 1980; 9:112–116.
21. Fedorov VV, Glukhov AV, Ambrosi CM, et al. Effects of KATP channel openers diazoxide and pinacidil in coronary-perfused atria and ventricles from failing and non-failing human hearts. J Mol Cell Cardiol. 2011; 51:215–225. [PubMed: 21586291]
22. Toal S, Farid TA, Selvaraj R. Short-term memory and restitution during ventricular fibrillation in human hearts: an in vivo study. Circ Arrhythm Electrophysiol. 2009; 2:562–570. [PubMed: 19843925]
23. Ogbaghebriel A, Shrier A. Differential responsiveness of atrial and ventricular myocytes to potassium channel openers. J Cardiovasc Pharmacol. 1995; 25:65–74. [PubMed: 7723355]
24. Panfilov AV. Is heart size a factor in ventricular fibrillation? Or how close are rabbit and human hearts? Heart Rhythm. Jul.2006 3:862–864. [PubMed: 16818223]
25. Glukhov AV, Fedorov VV, Lou Q, et al. Transmural dispersion of repolarization in failing and nonfailing human ventricle. Circ Res. 2010; 106:981–991. [PubMed: 20093630]
26. Baher AA, Uy M, Xie F, Garfinkel A, Qu Z, Weiss JN. Bidirectional ventricular tachycardia: ping pong in the His-Purkinje system. Heart Rhythm. 2011; 8:599–605. [PubMed: 21118730]
27. Pandit SV, Kaur K, Zlochiver S, et al. Left-to-right ventricular differences in I(KATP) underlie epicardial repolarization gradient during global ischemia. Heart Rhythm. Nov.2011 8:1732–1739. [PubMed: 21723845]

NIH-PA Author Manuscript
NIH-PA Author Manuscript
NIH-PA Author Manuscript

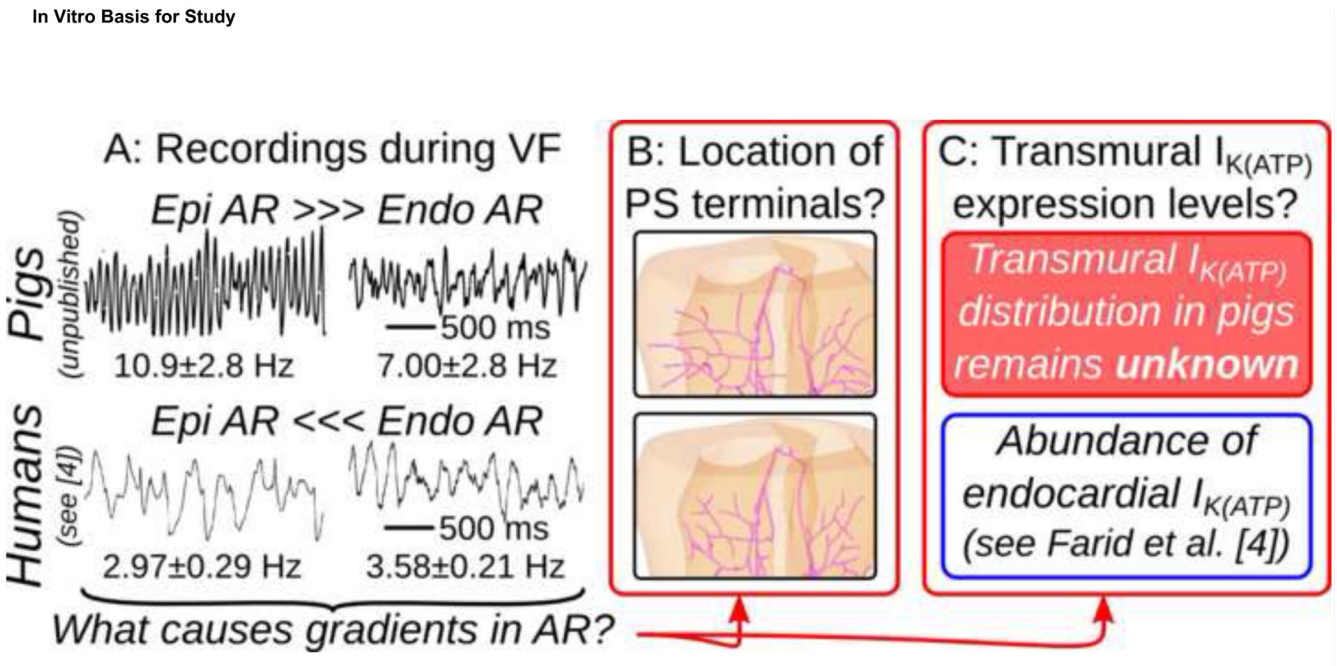

Figure 1.

(A):Epi/endo electrocardiograms during induced VF in Langendorff-perfused hearts showing transmural ΔAR. Human data were collected during a previous study.[4] Transmural AR differences in swine showed a strong epicardial-to-endocardial trend (too few samples for significance); human ΔAR was statistically significant (P=0.01).[4] Detailed methods for electrogram recordings can be found in the Online Supplement. (B): Schematics showing pig vs. human PS terminal locations. (C): Known information regarding transmural differences in $I_{K(ATP)}$ expression levels.

NIH-PA Author Manuscript

NIH-PA Author Manuscript

NIH-PA Author Manuscript

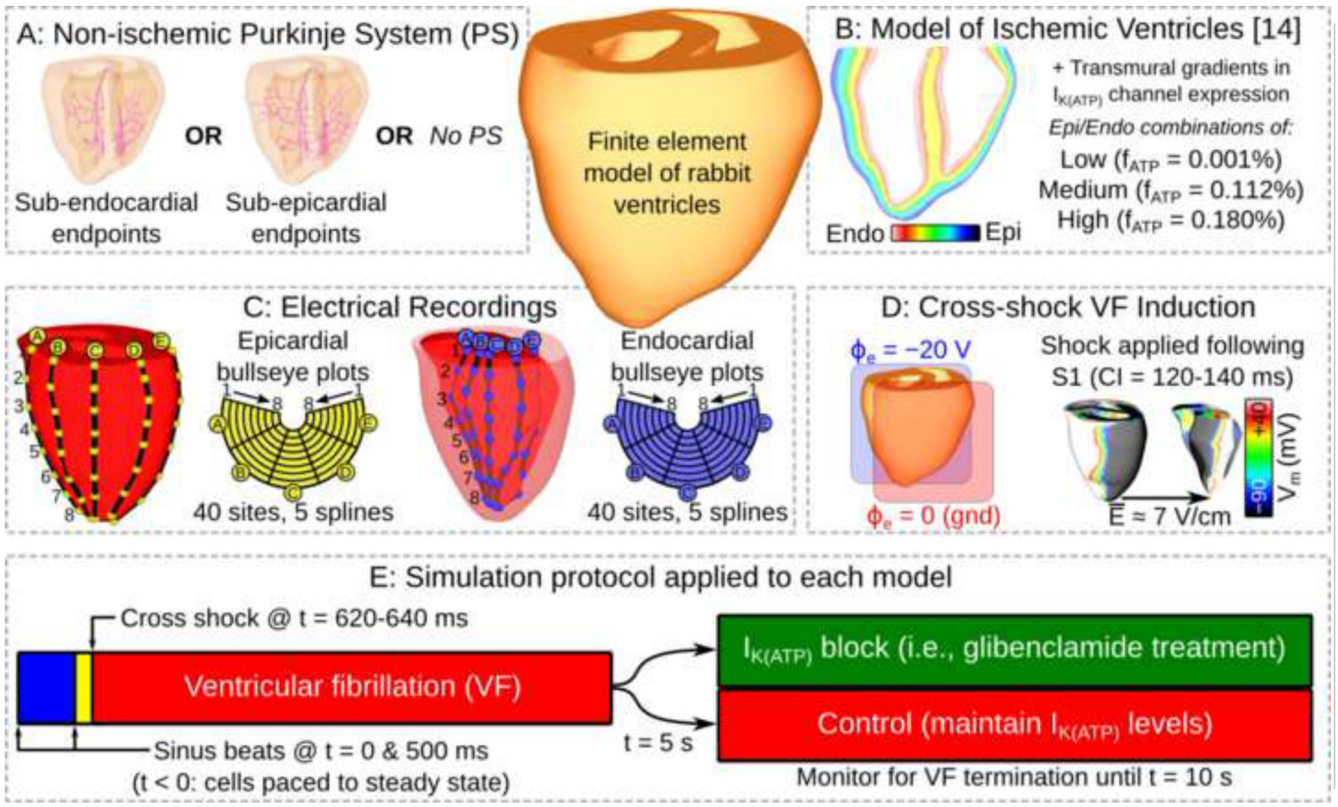

Figure 2.

(A): Different possibilities for PS model. (B): Transmural $I_{K(ATP)}$ gradients. (C): Experimentally motivated electrode configurations. (D): Cross-shock methodology for inducing VF. (E): Simulation protocol for VF initiation and simulated pharmacological treatment/control. CI: coupling interval; f_{ATP}: fraction of active $I_{K(ATP)}$ channels; V_m: transmembrane voltage.

NIH-PA Author Manuscript

NIH-PA Author Manuscript

NIH-PA Author Manuscript

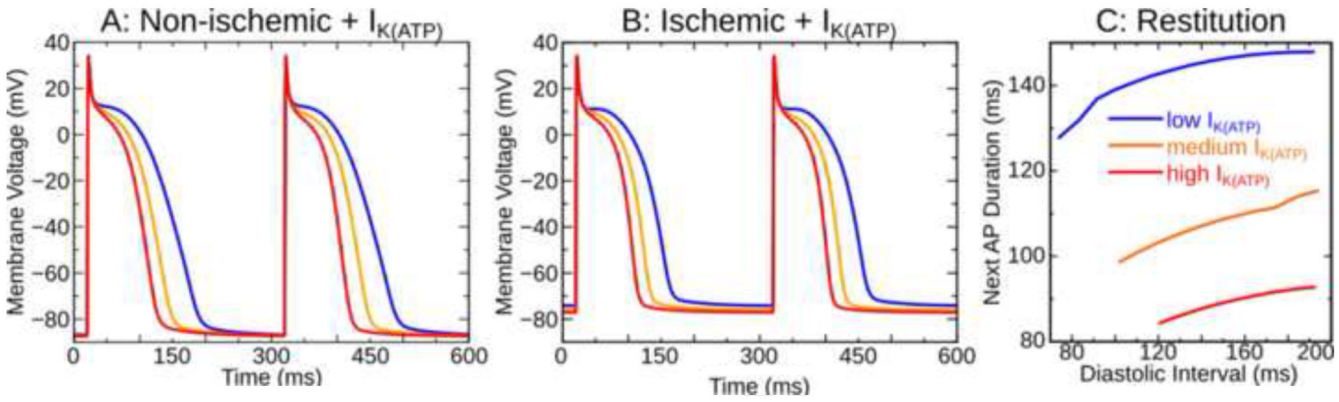

Figure 3.

APs in non-ischemic (A) and ischemic (B) ventricular myocytes with three $I_{K(ATP)}$ levels; $I_{K(ATP)}$ effects on the dynamic restitution relationship with ischemia are also highlighted (C). AP: action potential.

NIH-PA Author Manuscript

NIH-PA Author Manuscript

NIH-PA Author Manuscript

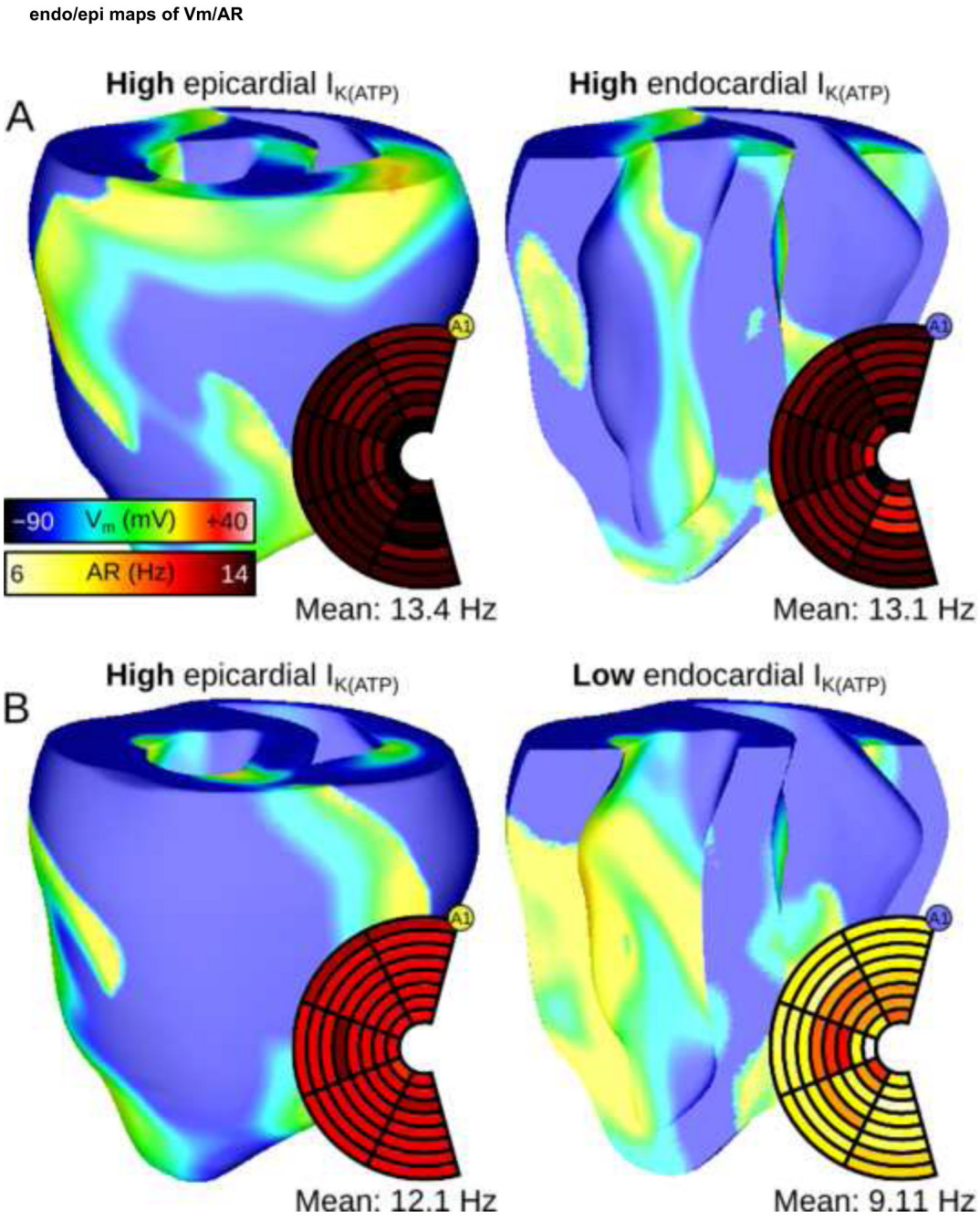

Figure 4.

(A&B): Spatial V_m maps with AR bull's eye plots inset (endocardial views: posterior wall cutaway). The high-to-low $I_{K(ATP)}$ gradient (B) causes ΔAR=2.99Hz. Electrode A1 is indicated for bull's eye plot orientation (see Fig. 2C). Supplementary Movies 1&2 show full V_m sequences for both examples.

NIH-PA Author Manuscript

NIH-PA Author Manuscript

NIH-PA Author Manuscript

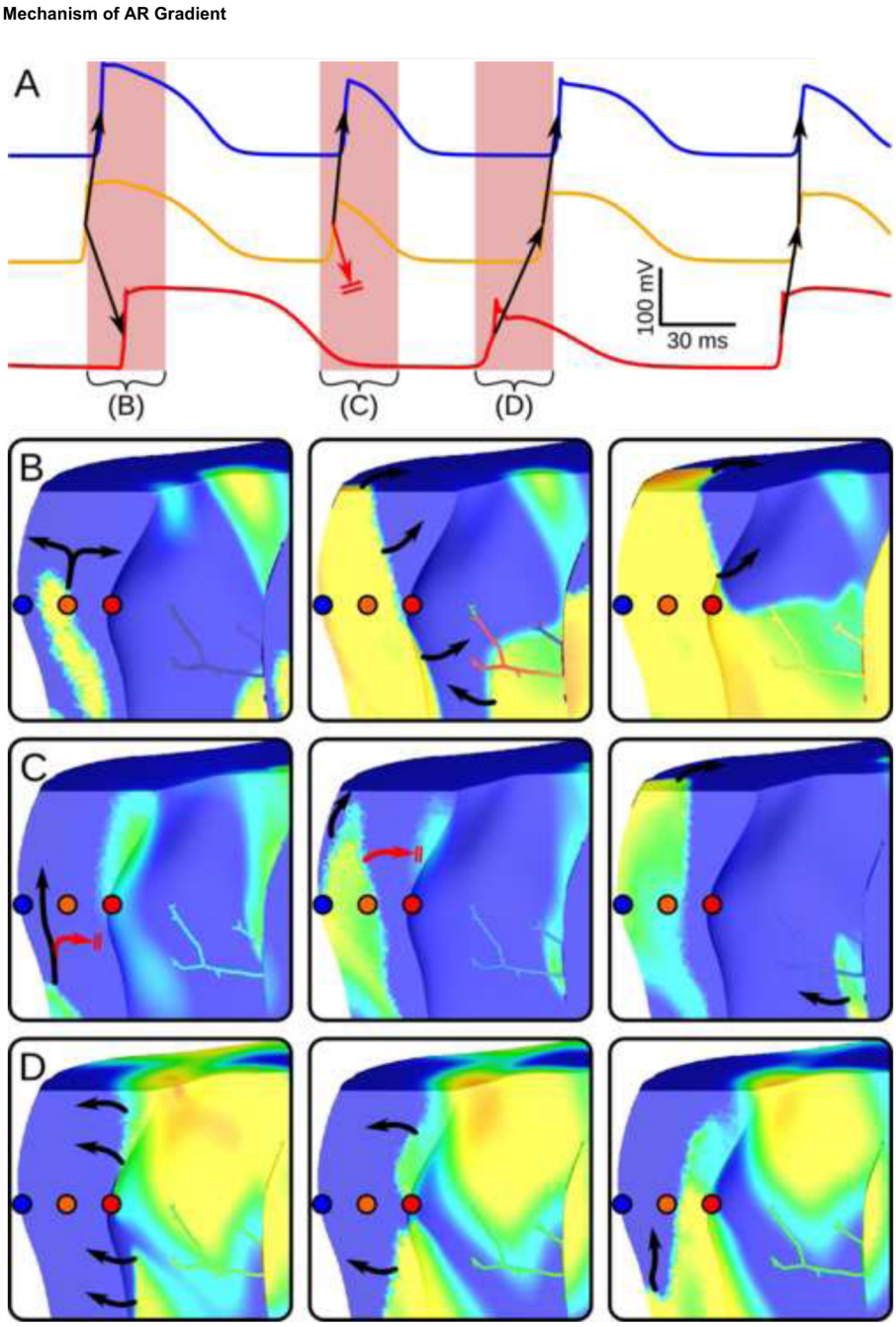

Figure 5.

(A): V_m recordings from 3 points, shown spatially in (B), for model with high-$I_{K(ATP)}$ epicardium, low-$I_{K(ATP)}$ endocardium, and sub-endocardial PS endpoints. Arrows indicate wavefront propagation, with conduction block indicated by double lines. V_m snapshots for highlighted intervals are shown in B-D (10*ms* between snapshots; same V_m scale as Fig. 4). (B): Excitation propagates from the midmyocardium towards both surfaces. (C): Conduction to low-$I_{K(ATP)}$ endocardium blocks due to intrinsically longer APs. (D): Activation proceeds from recovered endocardium to epicardium.

NIH-PA Author Manuscript
NIH-PA Author Manuscript
NIH-PA Author Manuscript

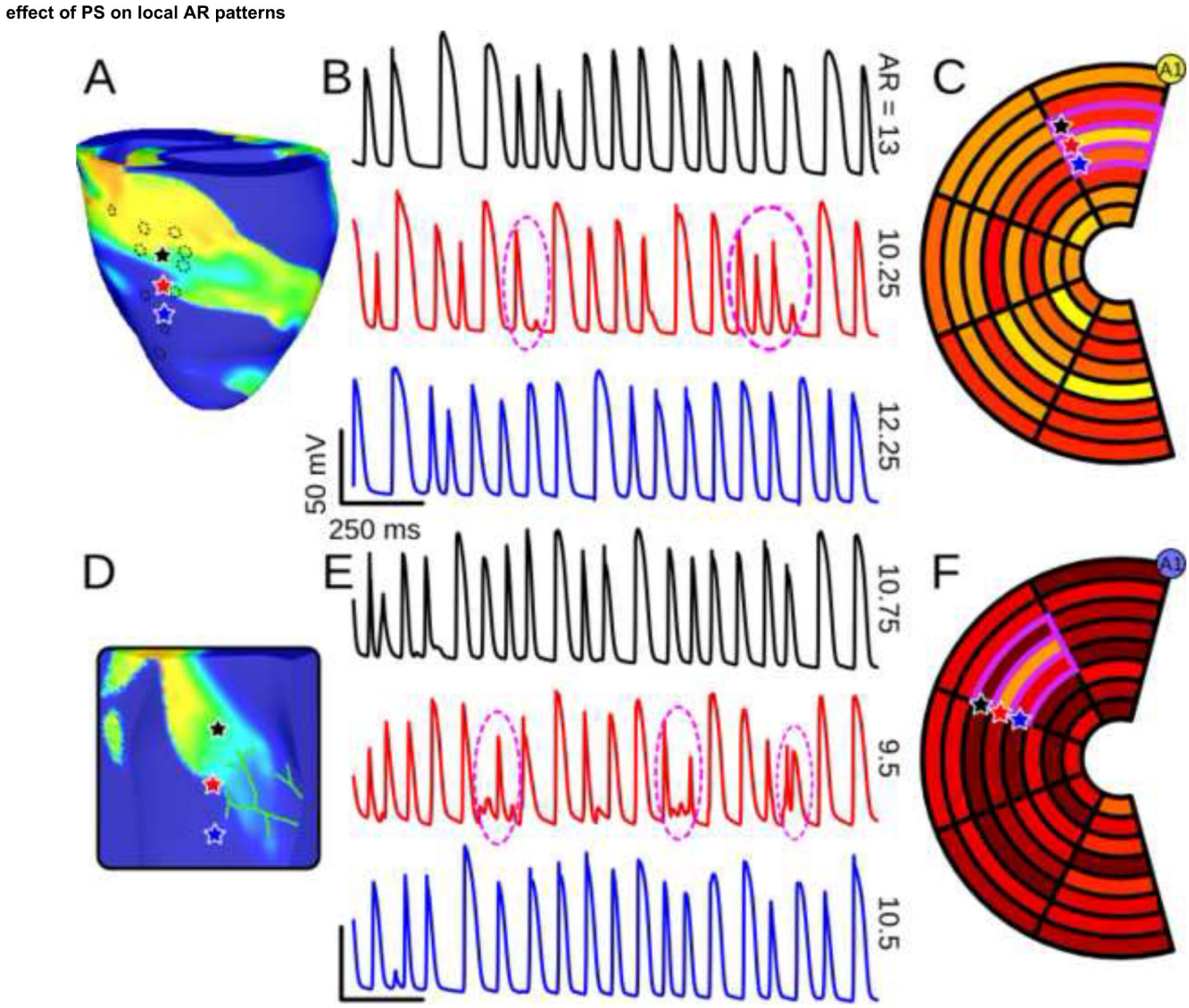

Figure 6.

(A): V_m snapshot with 3 highlighted epicardial recording sites; from the model with medium-$I_{K(ATP)}$ epicardium, low-$I_{K(ATP)}$ endocardium, and sub-epicardial PS. Dashed circles show approximate locations of PS endpoints. (B): V_m recordings from the 3 sites indicated in (A), matched by color. Intervals where AR was reduced due to PS activity are highlighted (dashed circles). (C): Epicardial AR plot (same scale as Fig. 4) for the model from (A) showing spatial disorganization (Moran's I=−0.00831). (D-F): Same as (A-C) but for the model with high-$I_{K(ATP)}$ endocardium, low-$I_{K(ATP)}$ epicardium, and sub-endocardial PS (visible in (D)). For endocardial AR plot in (F), Moran's I=−0.0798). Electrode A1 is indicated for bull's eye plot orientation (see Fig. 2C). Supplementary Movies 3&4 show full V_m sequences for both examples.

NIH-PA Author Manuscript

NIH-PA Author Manuscript

NIH-PA Author Manuscript

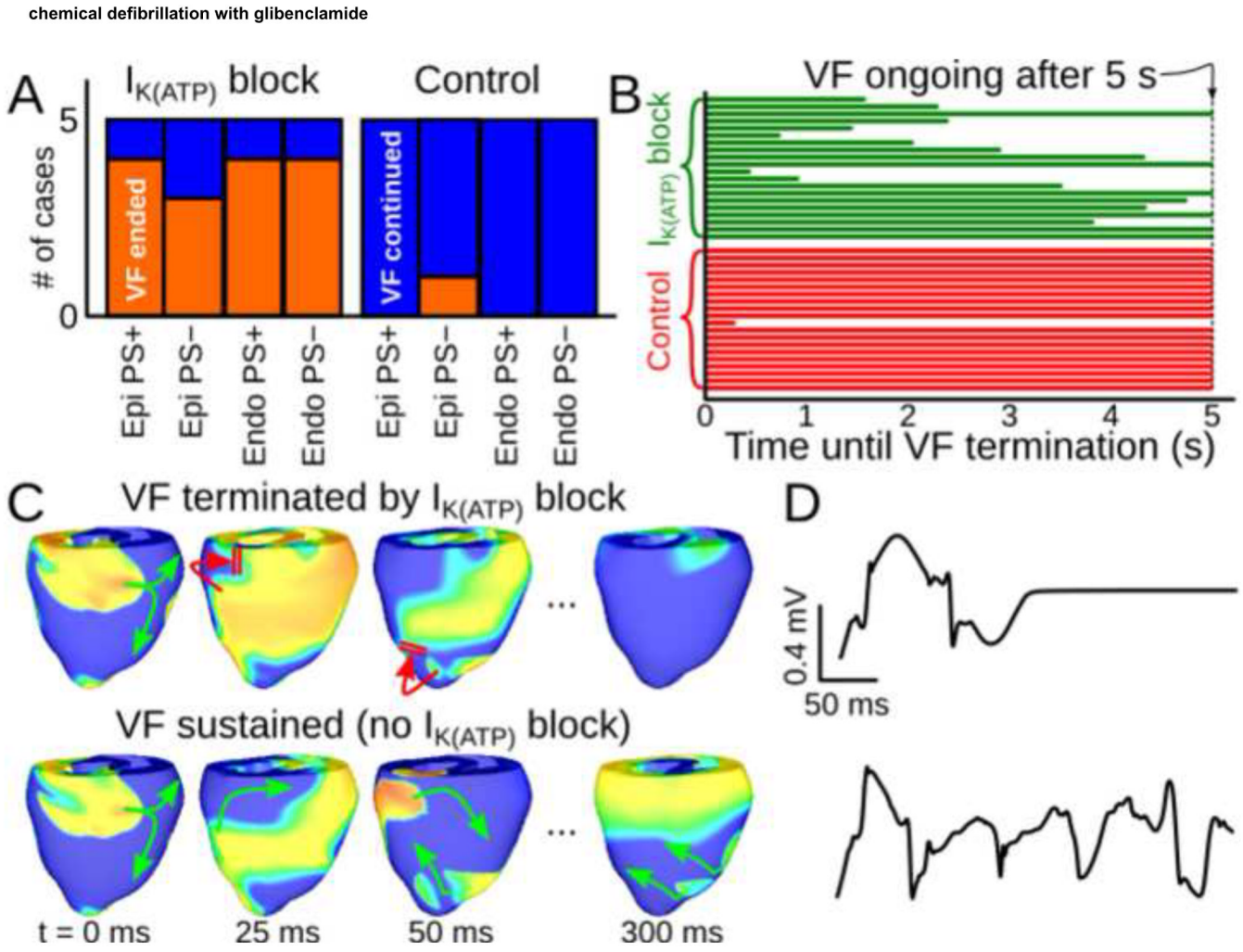

Figure 7.

:(A) Results of simulated glibenclamide application (left) vs. control (right) in all models. (B) Time to spontaneous VF termination for all models. (C): V_m maps (same scale as Fig. 4) showing VF termination in a model with $I_{K(ATP)}$ block (top) and persistent VF in an identical simulation but without $I_{K(ATP)}$ block (bottom). Green and red arrows show successful and failed wavefront propagation, respectively. (D): Pseudo-ECG lead I signals associated with sequences from (C).

NIH-PA Author Manuscript

NIH-PA Author Manuscript

NIH-PA Author Manuscript

Table 1

ARs during early VF for all models; ΔAR is epicardial-to-endocardial percent difference for Epi-PS models or endocardial-to-epicardial for Endo-PS models. PS: Purkinje system; Epi-PS: sub-epicardial PS; Endo-PS: sub-endocardial PS; $I_{K(ATP)}$: ATP-sensitive K^+ current; VF: ventricular fibrillation; AAR: activation rate gradient.

	$I_{K(ATP)}$		Without PS			With PS		
	Epi	**Endo**	**AR_{Epi}**	**AR_{Endo}**	**ΔAR**	**AR_{Epi}**	**AR_{Endo}**	**ΔAR**
Epi-PS	*Low*	*Low*	*Non-sustained VF*			*Non-sustained VF*		
	Med	*Low*	**10.3**	**8.57**	**16.9%**	**9.81**	**7.93**	**19.2%**
	High	*Low*	**10.8**	**8.71**	**19.4%**	**12.1**	**9.11**	**24.6%**
	Med	*Med*	11.4	11.1	3.12%	11.3	11.1	1.00%
	High	*Med*	12.6	11.9	5.67%	11.9	11.6	2.83%
	High	*High*	13.3	13.1	1.56%	13.4	13.1	2.74%
Endo-PS	*Low*	*Low*	*Non-sustained VF*			*Non-sustained VF*		
	Low	*Med*	**8.20**	**9.67**	**15.2%**	**8.04**	**9.54**	**15.7%**
	Low	*High*	**8.61**	**11.3**	**24.0%**	**8.41**	**10.9**	**22.8%**
	Med	*Med*	10.7	10.3	3.65%	10.4	10.3	1.09%
	Med	*High*	11.1	11.6	4.64%	11.3	11.9	4.58%
	High	*High*	12.7	12.2	3.93%	12.9	12.6	2.17%